oxidative processes of catechols. It is apparent that under the conditions used in the synthesis, the process can be reasonably thought to proceed by successive one-electron-transfer steps (oxidation of the copper(II)–catecholate complex to copper–semiquinonate, followed by internal electron transfer within the product). In the overall process, according to Rogic and Demmin,[39,40] no dioxygen is required, since an additional cupric species (the bis(pyridine)cupric chloride in the synthetic procedure) is sufficient to act as on electron acceptor. The problem remains open about the factors determining the successive oxidation process that involves the cleavage of a carbon–carbon bond.

Acknowledgment. The financial support of the Ministry of Public Education and of the CNR is gratefully acknowledged.

Contribution from the Department of Chemistry, York University, North York (Toronto), Ontario, Canada M3J 1P3

Electrochemistry and Spectroelectrochemistry of 1,8-Naphthalene- and 1,8-Anthracene-Linked Cofacial Binuclear Metallophthalocyanines. New Mixed-Valence Metallophthalocyanines

Nagao Kobayashi,*[,1] Herman Lam, W. Andrew Nevin,[2] Pavel Janda,[3] Clifford C. Leznoff,* and A. B. P. Lever*

Received March 20, 1990

1,8-Naphthalene- or 1,8-anthracene-linked cofacial dizinc, dicopper, and dicobalt diphthalocyanines have been studied by solution and surface electrochemistry, spectroelectrochemistry, and electron spin resonance (ESR). These derivatives are mixtures of syn and anti isomers that have very similar electrochemistry except where we comment specifically. The phthalocyanine ring first oxidation Pc(−1)/Pt(−2), the Co(III)/Co(II), and the Co(II)/Co(I) redox couples split into two couples as a consequence of intra-ring exchange interactions. The spectra of the electrochemically oxidized or reduced species and, in particular, those of the mixed-valence species are recorded. Exciton coupling energies are derived and are seen to be related to the ground-state mixed-valence splitting energies. These are discussed in terms of structure and inter-ring distance. Cobalt derivatives immobilized onto ordinary pyrolytic graphite catalyze the electroreduction of oxygen by two electrons to hydrogen peroxide.

Introduction

There is considerable interest in the electrochemistry and spectroelectrochemistry of binuclear metalloporphyrins[4–7] and binuclear[8–10] and polynuclear[8d,g,9,10] metallophthalocyanines. When two macrocyclic units are spaced closely to each other, properties that are not seen in mononuclear units often emerge. Most striking of these is the splitting of some redox couples, generating mixed-valence species whose properties have been discussed for several systems.[4,6,7c,8a,b,g,10] Mixed-valence behavior has been observed with some zinc derivatives of flexible clamshell phthalocyanines,[8g] but not with analogous cobalt derivatives.

We report the electrochemical and spectroelectrochemical properties of rigidly linked 1,8-naphthalene- and 1,8-anthracene-bridged cofacial binuclear metallophthalocyanines

(1) Visiting Professor from the Pharmaceutical Institute, Tohoku University, Sendai 980, Japan.

(2) Current address: Central Research Laboratories, Kanegafuchi Chemical Industry Co. Ltd., 2-80, 1-Chome, Yoshida-cho, Hyogo-ku, Kobe 652, Japan.

(3) Visiting research associate from the Heyrovsky Institute of the Czech Academy of Sciences, Prague, Czechoslovakia.

(4) (a) Mest, Y. L.; L'Her, M.; Collman, J. P.; Kim, K.; Helm, S.; Hendricks, N. H. *J. Electroanal. Chem. Interfacial Electrochem.* **1987**, *234*, 277; **1987**, *220*, 247. (b) Collman, J. P.; Prodolliet, W.; Leidner, R. *J. Am. Chem. Soc.* **1986**, *10*,, 2916. (c) Le Mest, Y.; Courtot-Coupez, J.; Collman, J. P.; Evitt, E. R.; Bencosme, C. S. *J. Electroanal. Chem. Interfacial Electrochem.* **1985**, *184*, 331. (d) Collman, J. P.; Marrocco, M.; Elliot, C. M.; L'Her, M. L. *J. Electroanal. Chem. Interfacial Electrochem.* **1981**, *124*, 113. (e) Collman, J. P.; Kim, K.; Leidner, C. R. *Inorg. Chem.* **1987**, *26*, 1152. (f) Ngameni, E.; Le Mest, Y.; L'Her, M.; Collman, J. P.; Hendricks, N. H.; Kim, K. *J. Electroanal. Chem. Interfacial Electrochem.* **1987**, *220*, 247.

(5) Cowan, J. A.; Saunders, J. K. M. *J. Chem. Soc., Perkin Trans. 1* **1987**, 2395.

(6) (a) Crossley, M. J.; Burn, P. L. *J. Chem. Soc., Chem. Commun.* **1987**, 39. (b) Buchler, J. W.; Elsasser, K. *Angew. Chem., Int. Ed. Engl.* **1986**, *25*, 286. (c) Williams, R. F. X.; White, D.; Hambright, P.; Schamin, A.; Little, R. G. *J. Electroanal. Chem. Interfacial Electrochem.* **1983**, *110*, 69. (d) Becker, J. Y.; Dolphin, D.; Paine, J. B. Wijesekera, T. J. *J. Electroanal. Chem. Interfacial Electrochem.* **1984**, *164*, 335.

(7) Bottomley, L. A.; Gorce, J.-N.; Landrum, J. T. *Inorg. Chim. Acta* **1986**, *125*, 135. (b) Kadish, K. M.; Cheng, J. S.; Cohen, I. A.; Summerville, D. *ACS Symp. Ser.* **1977**, *No. 38*, 65. (c) Kadish, K. M.; Larson, G.; Lexa, D.; Momenteau, M. *J. Am. Chem. Soc.* **1975**, *97*, 282.

(8) (a) Leznoff, C. C.; Lam, H.; Nevin, W. A.; Kobayashi, N.; Janda, P.; Lever, A. B. P. *Angew. Chem., Int. Ed. Engl.* **1987**, *26*, 1021. (b) Leznoff, C. C.; Lam, H.; Marcuccio, S. M.; Nevin, W. A.; Janda, P.; Kobayashi, N.; Lever, A. B. P. *J. Chem. Soc., Chem. Commun.* **1987**, 699. (c) Nevin, W. A.; Hempstead, M. R.; Liu, W.; Leznoff, C. C.; Lever, A. B. P. *Inorg. Chem.* **1987**, *26*, 570. (d) Nevin, W. A.; Liu, W.; Greenberg, S.; Hempstead, M. R.; Marcuccio, S. M.; Melnik, M.; Leznoff, C. C.; Lever, A. B. P. *Inorg. Chem.* **1987**, *26*, 891. (e) Liu, W.; Hempstead, M. R.; Nevin, W. A.; Melnik, M.; Lever, A. B. P.; Leznoff, C. C. *J. Chem. Soc., Dalton Trans.* **1987**, 2511. (f) Minor, P. C.; Lever, A. B. P. *Inorg. Chem.* **1983**, *22*, 826. (g) Manivannan, V.; Nevin, W. A.; Leznoff, C. C.; Lever, A. B. P. *J. Coord. Chem.* **1988**, *19*, 139. (h) Leznoff, C. C.; Greenberg, S.; Marcuccio, S. M.; Minor, P. C.; Seymour, P.; Lever, A. B. P.; Tomer, K. B. *Inorg. Chim. Acta* **1984**, *89*, L35.

(9) (a) Simic-Glavaski, B.; Tanaka, A. A.; Kenney, M. E.; Yeager, E.; *J. Electroanal. Chem. Interfacial Electrochem.* **1987**, *229*, 285. (b) Mezza, T. M.; Armstrong, N. R.; Kenney, M. *J. Electroanal. Chem. Interfacial Electrochem.* **1984**, *176*, 259. (c) Mezza, T. M.; Armstrong, N. R.; Ritter, G. W.; Iafalice, J. P.; Kenney, M. E. *J. Electroanal. Chem. Interfacial Electrochem.* **1982**, *137*, 227.

(10) Wheeler, B. L.; Nagasubramanian, G.; Bard, A. J.; Schechtman, L. A.; Dininny, D. R.; Kenney, M. E. *J. Am. Chem. Soc.* **1984**, *106*, 7404. Anderson, A. B.; Gordon, T. L.; Kenney, M. E. *J. Am. Chem. Soc.* **1985**, *107*, 192. DeWulf, D. W.; Leland, J. K.; Wheeler, B. L.; Bard, A. J.; Batzel, D. A.; Dininny, D. R.; Kenney, M. E. *Inorg. Chem.* **1987**, *26*, 266.

0020-1669/90/1329-3415$02.50/0

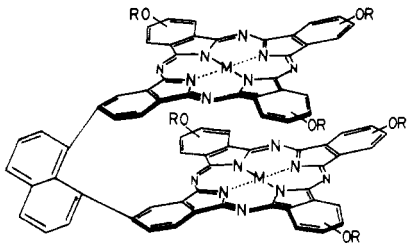

Nap[ZnTrNPc]$_2$: M=Zn, R=$CH_2C(CH_3)_3$
Nap[CoTrNPc]$_2$: M=Co, R=$CH_2C(CH_3)_3$
Nap[CuTrNPc]$_2$: M=Cu, R=$CH_2C(CH_3)_3$

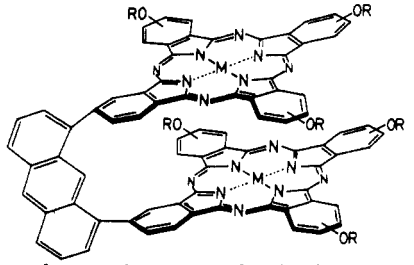

Ant[ZnTrNPc]$_2$: M=Zn, R=$CH_2C(CH_3)_3$
Ant[CoTrNPc]$_2$: M=Co, R=$CH_2C(CH_3)_3$

Figure 1. Naphthalene- and anthracene-linked cofacial binuclear metallophthalocyanines used in the present study. "Syn" structures are shown.

(Figure 1), to explore their exchange interactions and capacity for mixed-valence species formation. As shown below, interactions in the pillared phthalocyanines are larger than in the corresponding porphyrins, and the formation of mixed-valence redox states is observed. In contrast to the flexible clamshell species, cobalt complexes of these pillared species do exhibit mixed-valence behavior both at the cobalt atom and at the phthalocyanine ring. This is the first detailed study of the mixed-valence behavior of transition-metal metallophthalocyanine species.

In addition, we describe the catalytic behavior of the cobalt derivatives for the electroreduction of oxygen, since several cofacial cobalt porphyrins are known to function as excellent catalysts for this reaction.[11,12]

While phthalocyanines have traditionally been important to the pigment, paint, and ink industry, they are also now employed as the photoconductive layer in photocopying equipment. Moreover, their unusual chemical stability, coupled with their intense color and redox activity, is leading to considerable worldwide interest in developing more high-technology applications. These include electrochromic devices, chemical sensors, molecular metals, laser dyes, optical disks, photovoltaic cells, fuel cells, etc., as well as applications in medicine, such as photodynamic cancer therapy.[13] Mixed-valence species are likely to be of value in some of these applications, and thus such studies have both fundamental and potential industrial benefit over a wide field.

Experimental Section

The synthesis, purification, and characterization of the naphthalene[8a,14] (Nap[MTrNPc]$_2$-) and anthracene- (Ant[MTrNPc]$_2$-) linked[14] binuclear phthalocyanines and mononuclear metallotetraneopentoxyphthalocyanines[15] (MTNPcs) are described elsewhere. *N,N*-Dimethylformamide (DMF) (Aldrich, Gold Label, anhydrous, H_2O <0.005%, packed under nitrogen), and *o*-dichlorobenzene (DCB) (Aldrich, Gold Label) were used as supplied. Tetrabutylammonium perchlorate (TBAP) (Kodak) was recrystallized from absolute ethanol and dried at 50 °C under vacuum for 2 days.

Electronic spectra were recorded with a Perkin-Elmer Hitachi Model 340 microprocessor spectrometer. Cyclic and differential-pulse voltammetries were performed with a Princeton Applied Research (PARC) 174A polarographic analyzer coupled to a PARC 175 universal programmer. Electrochemical data were recorded under an atmosphere of nitrogen, or argon, by using a conventional three-electrode cell. A platinum disk described by the cross-sectional area of a 27-gauge wire (area· 10^{-3} cm^2), sealed in glass, was used as the working electrode, a platinum wire served as the counter electrode, and the reference electrode was Ag/AgCl (−0.045 V vs SCE)[16] (in saturated KCl, separated by a frit) corrected for junction potentials by being referenced internally to the ferrocenium/ferrocene (Fc^+/Fc) couple. In various experiments involving DMF solutions, the Fc^+/Fc couple was seen to lie in the range +0.35 to +0.45 V vs Ag/AgCl/Cl^-, due to variations in junction potentials. In DCB, the Fc^+/Fc couple was observed at approximately 0.59 V vs Ag/AgCl/Cl^-.[17]

All DMF solutions were prepared and measurements were made under an atmosphere of nitrogen within a Vacuum Atmospheres Drilab. The DCB solutions were prepared in air, degassed by repeated freeze–pump–thaw cycles, and then transferred to the drybox. The stability of the Ag/AgCl/Cl^- electrode was checked by using a solution of ferrocene in DCB; it was stable for at least 2 days. Spectroelectrochemical measurements were made with a 0.45-mm-path length optically transparent thin-layer electrode (OTTLE) cell, utilizing a gold minigrid (500 lines/in. 60% transmittance)[18] or with a 1-mm path length OTTLE utilizing a Pt minigrid,[19] in conjunction with the Hitachi Perkin-Elmer spectrometer.

Potential scans for oxygen reduction were performed with a Pine Instrument RD3 potentiostat and the rotating studies with a Pine Instrument PIR rotator. The working-electrode material for oxygen reduction studies is ordinary pyrolytic graphite (OPG), which has a circular area of 0.49 cm^2. Before each experiment, the OPG electrode surface was cleaned by successive polishings with 1.0, 0.3, and 0.005 μm alumina (Linde) suspended in water on a Metron polishing cloth. For the adsorption of the catalysts onto the OPG surface, the electrode was immersed in ca. (1–5) × 10^{-5} M phthalocyanine solution for ca. 10 min, removed from the solution, washed with ethanol and distilled water, and dried under reduced pressure. Judging from the cyclic voltammetric curve under argon at the prepared electrode, the surface concentration of the catalyst becomes steady state by an immersion of less than 10 min. The cell comprised a separate chamber for each electrode, with a Luggin capillary extending from the reference chamber to the proximity of the OPG surface. For the aqueous experiments, a saturated calomel electrode (SCE) and a large platinum plate were used as a reference and a counter electrode, respectively. Argon gas (Linde) was purified by passage through heated copper filings, anhydrous $CaSO_4$ (Drierite), molecular sieves (BDH 3A), and glass wool. Oxygen gas (Linde) was purified by passage through anhydrous $CaSO_4$, NaOH pellets (AnalaR), molecular sieves, and glass wool.

Solutions for electrochemistry and spectroelectrochemistry contained 0.1–0.3 M TBAP, as supporting electrolyte.

Electron spin resonance (ESR) data were obtained on a Varian E4 spectrometer, calibrated with diphenylpicrylhydrazide (DPPH). ESR spectra of electrochemically generated Nap[CoTrNPc]$_2$ species in the presence or absence of 2-methylimidazole were obtained by bulk electrolysis of a solution (degassed by freeze–pump–thaw cycles) under an atmosphere of nitrogen in the drybox and transferring the species to sealable ESR tubes. Control electronic spectra were also taken. The bulk electrolysis cell consisted of a platinum-plate working electrode, a Pt-flag counter electrode, and a silver-wire quasi-reference electrode. Counter

(11) (a) Collman, J. P.; Marrocco, M.; Denicevich, P.; Koval, C.; Anson, F. C. *J. Electroanal. Chem. Interfacial Electrochem.* **1979**, *101*, 117; *J. Am. Chem. Soc.* **1980**, *102*, 6027. (b) Durand, R. R.; Bencosme, C. S.; Collman, J. P.; Anson, F. C. *J. Am. Chem. Soc.* **1983**, *105*, 2694, 2710. (c) Collman, J. P.; Anson, F. C.; Bencosme, C. S.; Durand, R. R.; Kreh, R. P. *J. Am. Chem. Soc.* **1983**, *105*, 2699.
(12) (a) Liu, H. Y.; Weaver, M. J.; Wang, C. B.; Chang, C. K. *J. Electroanal. Chem. Interfacial Electrochem.* **1983**, *145*, 439. (b) Chang, C. K.; Liu, H. Y.; Abdalmuhdi, I. *J. Am. Chem. Soc.* **1984**, *106*, 2725. (c) Ni, C.-L.; Abdalmuhdi, I.; Chang, C. K.; Anson, F. C. *J. Phys. Chem.* **1987**, *91*, 1158. (d) Liu, H. Y.; Abdalmuhdi, I.; Chang, C. K.; Anson, F. C. *J. Phys. Chem.* **1985**, *89*, 665.
(13) Lever, A. B. P. *CHEMTECH* **1987**, *17*, 506–10. *The Phthalocyanines*; Leznoff, C. C., Lever, A. B. P., Eds.; VCH: New York, 1989.
(14) Lam, H.; Marcuccio, S. M.; Svirskaya, P. I.; Greenberg, S.; Lever, A. B. P.; Leznoff, C. C.; Zerny, C. *Can. J. Chem.* **1989**, *67*, 1087.
(15) Leznoff, C. C. Marcuccio, S. M.; Greenberg, S.; Lever, A. B. P.; Tomer, K. B. *Can. J. Chem.* **1985**, *63*, 623.
(16) Bard, A. J.; Faulkner, L. R. *Electrochemical Methods*; John Wiley: New York, 1980.
(17) The position of the ferrocenium/ferrocene couple is quite sensitive to the organic solvent employed: Gagne, R. R.; Koval, C. A.; Lisensky, D. C. *Inorg. Chem.* **1980**, *19*, 2854. Gritzner, G.; Kuta, J. *Electrochim. Acta* **1984**, *29*, 869. Bohling, D. A.; Evans, J. F.; Mann, K. R. *Inorg. Chem.* **1982**, *21*, 3546. Bagchi, R. N.; Bond, A. M.; Colton, R.; Luscombe, D. L.; Moir, J. E. *J. Am. Chem. Soc.* **1986**, *108*, 3352. Harman, W. D.; Sekine, M.; Taube, H. *J. Am. Chem. Soc.* **1988**, *110*, 5725.
(18) Nevin, W. A.; Lever, A. B. P. *Anal. Chem.* **1988**, *60*, 727.
(19) Kobayashi, N.; Nishiyama, Y. *J. Phys. Chem.* **1985**, *89*, 1167.

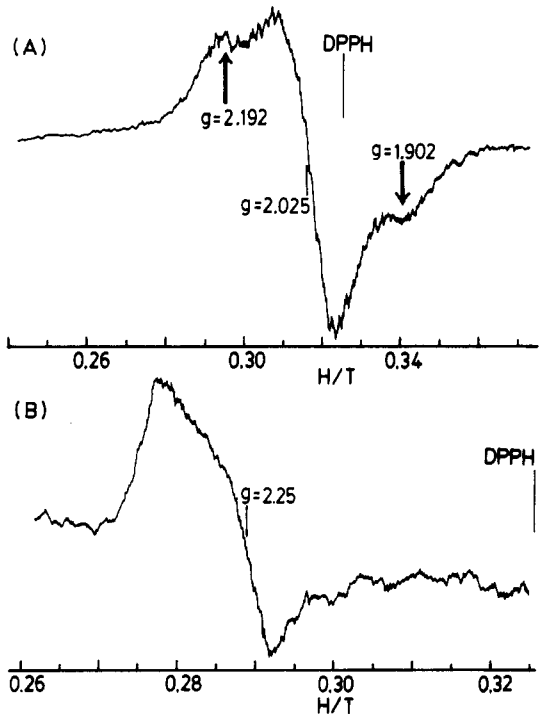

Figure 2. ESR spectra of (A) Nap[CuTrNPc]$_2$ in toluene and (B) Nap[Co^{II}TrNPc(−2)][Co^{I}TrNPc(−2)]$^-$ in the presence of 2-methylimidazole in DCB at 77 K. [Nap[CuTrNPc]$_2$]/M = 1 × 10^{-3}. [Nap[CoTrNPc]$_2$]/M = 2.6 × 10^{-4}. [2-Methylimidazole]/M = 2 × 10^{-3}. In part B, the solution contains 0.13 M TBAP.

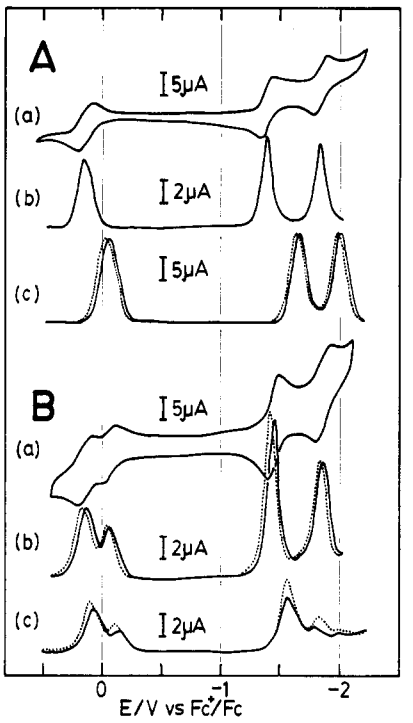

Figure 3. Cyclic and differential-pulse voltammograms of (A) ZnTNPc and (B) Ant[ZnTrNPc]$_2$ in DMF (curves a and b) and in DCB (curves c) at Pt-disk working electrode. Scan rates/mV s^{-1} = 100 for cyclic voltammetry and 5 for differential-pulse (DP) voltammetry. In DP diagrams, solid lines indicate cathodic scan and dotted lines anodic scan. [ZnTNPc]/M = ca. 1 × 10^{-3} in DMF and 3 × 10^{-3} in DCB. [Ant[ZnTrNPc]$_2$]/M = ca. 4 × 10^{-4} in DMF and 2.64 × 10^{-4} in DCB. [TBAP]/M = 0.3.

and reference electrodes were separated from the working compartment by medium glass frits.

Results and Discussion

Complex NMR absorptions of Nap[H$_2$TrNPc]$_2$ in the region of δ = 7.3–8.5 have been analyzed as an approximately 1:1 mixture of syn and anti isomers[8a,14] in the metal-free derivative. It is likely that all the metal complexes are also mixtures of syn and anti isomers, but the proportions may vary from 1:1. Each of the syn and anti isomers of Nap- or Ant[MTrNPc]$_2$ exists as a mixture of 36 regioisomers with respect to the neopentoxy substituent. Previous studies[8] of such regioisomer mixtures have indicated that they have essentially identical electrochemical and optical properties and are largely inseparable by chromatographic methods. The properties of the syn and anti isomers are, however, expected to be different, as further developed below.

(i) Electron Spin Resonance. Two Cu(II) (I = $^3/_2$) ions in close proximity frequently produce two strong perpendicular transitions, which may result in seven equally spaced lines in the g = 2 region of their ESR spectra.[20,21] The ESR spectrum of Nap[CuTrNPc]$_2$ shows (Figure 2A) a peak and a trough at g = 2.192 and 1.902, due to two perpendicular transitions by two equivalent and coupled Cu(II) ions in addition to a signal due to uncoupled Cu(II) ions (g = 2.025). A seven-line pattern did not appear. The mixed spectra obtained here stem from the presence of the syn and anti isomers which affect the Cu–Cu bond distance and are important to this analysis.

Accordingly, the signals at g = 2.192 and 1.902 are associated with the syn isomer, while the g = 2.025 signal is due to the anti isomer. It is impossible to evaluate the Cu–Cu distance from this spectrum, since the zero-field splitting parameters are not obtainable. However, judging from the X-ray crystallographic data on 1,8-diphenylnaphthalene whose two phenyl groups are forced apart from each other, the Cu–Cu distance in the syn form of this compound should be at least 4.3 Å. If CPK molecular models are used for this purpose, a rather larger value would result.[22,23]

The ESR spectra of the Nap[CoTrNPc]$_2$ species were recorded in DCB at 77 K. In the absence of an axial ligand, the ESR spectra of both Nap[Co^{II}TrNPc]$_2$ and its one-electron-reduced [Co^{II}TrNPcCo^{I}TrNPc]$^-$ species exhibited no signal. When 2-methylimidazole was added to the one-electron-reduced species, however, an ESR spectrum typical of a cobalt(II) center axially coordinated by a nitrogeneous base[11c] was obtained (Figure 2B), although its shape was slightly deformed (g = 2.25). Unfortunately, a clear hyperfine splitting of the parallel component, which would provide a clue as to whether a cobalt nucleus (I = $^7/_2$) is interacting with a nitrogen nucleus (I = 1) or with another cobalt nucleus, was not observed. The cause may be the presence of syn and anti isomers. We will show below that the one-electron-reduced species is a Nap[Co^{II}TrNPc][Co^{I}TrNPc]$^-$ mixed-valence compound.

(ii) Electrochemistry. In general, in the electrochemical data that follow, we describe either simultaneous two-electron processes where oxidation or reduction of the binuclear molecule occurs at the same potential in both rings or stepwise oxidations or reductions where mixed-valence species are generated by the sequential redox of each ring. Note that the simultaneous two-electron processes will have the characteristics of a one-electron process, but with twice the current.[16] Further, the assignment of mixed-valence products may not always be unequivocally determined by the

(20) Chikira, M.; Yokoi, H.; Isobe, T. *Bull. Chem. Soc. Jpn.* **1974**, *47*, 2208. Chikira, M.; Kon, H.; Hawley, R. A.; Smith, K. M. *J. Chem. Soc., Dalton Trans.* **1979**, 246 and some references cited therein. Chasteen, N. D.; Belford, R. L. *Inorg. Chem.* **1970**, *9*, 169.

(21) Kobayashi, N.; Lever, A. B. P. *J. Am. Chem. Soc.* **1987**, *109*, 7433.

(22) This Cu–Cu distance is considerably larger than the distance between the 1- and 8-positions of naphthalene (ca. 2.5 Å).[23a] The CPK model also suggests that the two phthalocyanine planes are stretching apart from each other, because the 1- and 8-positions of naphthalene are too close for them to be attached. In the 1,8-anthracene-linked diphthalocyanine series, such a phenomenon should not take place. Accordingly, the Cu–Cu distance in the syn isomer is considered to be approximately equal to the distance between the 1- and 8-positions of anthracene (ca. 4.95 Å).[23b]

(23) (a) House, H. O.; Koepsell, D. G.; Campbell, W. J. *J. Org. Chem.* **1972**, *37*, 1003. (b) Fillers, J. P.; Ravichandran, K. G.; Abdalmuhdi, I.; Chang, C. K. *J. Am. Chem. Soc.* **1986**, *108*, 417.

Table I. Electrochemical Data for Mononuclear and Binuclear Zinc and Copper Derivatives

couple	DCB solution $E_{1/2}$/V[a]	DCB solution ΔE_p/mV[b]	DMF solution $E_{1/2}$/V[a]	DMF solution ΔE_p/mV[b]
ZnTNPc System				
Pc(0)/Pc(-1)	0.64[c,d]			
Pc(-1)/Pc(-2)	-0.02	120	0.05[e]	85
Pc(-2)/Pc(-3)	-1.66	110	-1.43	95
Pc(-3)/Pc(-4)	-2.04	65	-1.85	95
Ant[ZnTrNPc]$_2$ System				
[Pc(-1)]$_2$/[Pc(-1)Pc(-2)]	0.08	(70)	0.16	(85)
[Pc(-1)Pc(-2)]/[Pc(-2)]$_2$	-0.13	(80)	-0.05	(75)
[Pc(-2)]$_2$/[Pc(-2)Pc(-3)]	-1.54[f]	100		
[Pc(-2)]$_2$/[Pc(-3)]$_2$			-1.41	70
[Pc(-2)Pc(-3)]/[Pc(-3)]$_2$	-1.80[g]	110		
[Pc(-3)]$_2$/[Pc(-4)]$_2$			-1.93	60
Nap[ZnTrNPc]$_2$ System				
[Pc(0)]$_2$/[Pc(-1)]$_2$?	0.73[f]		0.71[g]	80
[Pc(-1)]$_2$/[Pc(-1)Pc(-2)]	0.07	(50)	0.19	(80)
[Pc(-1)Pc(-2)]/[Pc(-2)]$_2$	-0.14	(50)	0.01	(70)
[Pc(-2)]$_2$/[Pc(-3)]$_2$	-1.67, -1.83[d]	(70)	-1.47	100
[Pc(-3)]$_2$/[Pc(-4)]$_2$	-2.02[d]	110	-1.85	70
Nap[CuTrNPc]$_2$[h] System				
[Pc(0)]$_2$/[Pc(-1)]$_2$?	0.74[g]			
[Pc(-1)]$_2$/[Pc(-1)Pc(-2)]	0.27	(50)		0.41[d]
[Pc(-1)Pc(-2)]/[Pc(-2)]$_2$	0.07	(50)		0.11[d]
[Pc(-2)]$_2$/[Pc(-3)]$_2$	-1.58	60	-1.28	50
[Pc(-3)]$_2$/[Pc(-4)]$_2$	-1.89	80	-1.72	60

[a] Potentials are reported with respect to the ferrocenium/ferrocene couple. $E_{1/2}$ values were measured by cyclic voltammetry at 200, 100, 50, and 20 mV/s. Average data $E = (E_{pa} + E_{pc})/2$ are reported. Data in parentheses are estimated from overlapping waves. [b] Values of $\Delta E_p = (E_{pa} - E_{pc})$ are given at a potential sweep rate of 50 mV/s. [c] Data from ref 8g. [d] Potentials are approximate because the waves are weak or broad. Reported values of $E_{1/2}$ were obtained by differential-pulse voltammetry. [e] The position of this wave shifts to higher potential in more concentrated solutions. These data were collected in solutions of approximately 10^{-4} M. [f] Assignment of these couples is tentative. Because of instability at high potentials, spectroelectrochemistry could not be performed to confirm these assignments. [g] Irreversible couple. [h] This compound displayed a weak extra couple at -1.75 or -1.52 V in DCB or DMF, respectively.

electrochemical data in the sense that additional waves could conceivably have arisen from impurity or decomposition products. However all the mixed-valence species have been characterized by spectroelectrochemistry, described below, and thus the electrochemical assignments are secure.

(a) Zinc and Copper Derivatives. Figure 3 shows typical cyclic and/or differential-pulse voltammograms (CV and DPV respectively) of ZnTNPc and Ant[ZnTrNPc]$_2$ in DMF or DCB. Data on mononuclear ZnTNPc[8g] are shown here for comparison. Redox assignments are based on this mononuclear ZnTNPc control data (Table I). Ant[ZnTrNPc]$_2$ gave two oxidation and two reduction couples in DMF, corresponding in potential to two quasi-reversible one-electron reductions and one quasi-reversible one-electron oxidation of the phthalocyanine ring ($i_a = i_c$, $i \propto v^{1/2}$). From the amount of current in the cyclic voltammogram and/or the area of the peaks in the DPV voltammogram, the two reduction waves involve two electrons each, per binuclear molecule, while the two oxidation couples are associated with approximately one electron each, per binuclear molecule.

Similar behavior has been reported for a flexible zinc phthalocyanine binuclear molecule linked by a five-atom bridge, EtMeO(5)[ZnTrNPc]$_2$,[8g] where EtMeO(5) represents an (-OCH$_2$C(Me)(Et)CH$_2$O-) bridge. In that case, controlled-potential electrochemistry confirmed that the first and second oxidation waves arose through the stepwise oxidation of the two phthalocyanine rings,[8g] i.e. Pc(-2)Pc(-2) → Pc(-2)Pc(-1) → Pc(-1)Pc(-1).[24] The two oxidation waves observed with Ant-

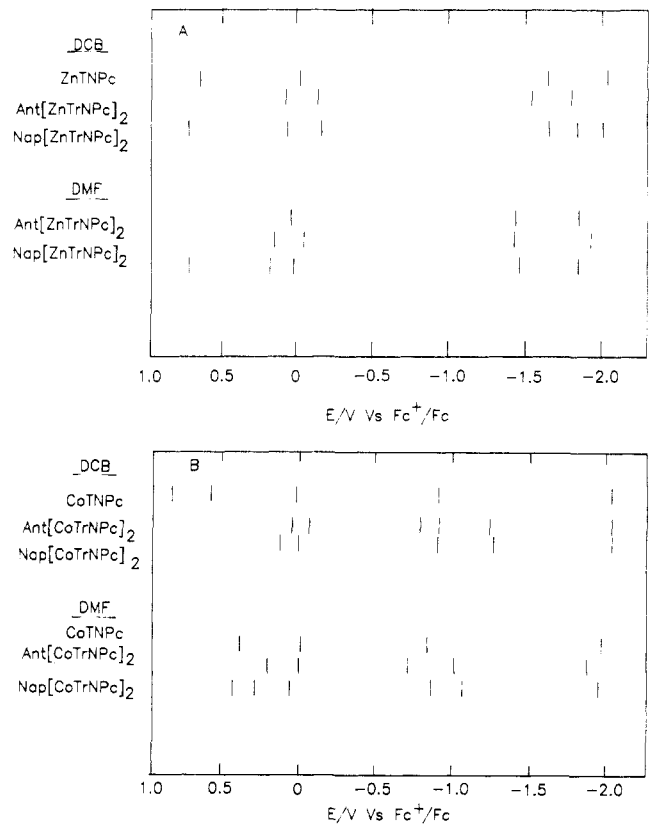

Figure 4. Schematic stick representation of redox couple potentials in MTNPc, and the anthracene and naphthalene species: (A) for zinc; (B) for cobalt.

[ZnTrNPc]$_2$, are similarly assigned since oxidation to the doubly oxidized Pc(0) level lies at a much more positive potential.[8c-g] Ring oxidation of the monomeric species lies at a potential lying between the two ring oxidation potentials of the cobalt and zinc binuclear species. Similar behavior is observed in the binuclear μ-oxo-bridged silicon phthalocyanine,[9c] compared with the mononuclear species.

In DCB, all the redox couples of ZnTNPc (Figure 3A(c)) and Ant[ZnTrNPc]$_2$ (Figure 3B(c)) lie negative of those in DMF. However as in DMF, the first ring oxidation of two phthalocyanine units in Ant[ZnTrNPc]$_2$ in DCB proceeded in a stepwise fashion, with potential separation of ca. 210 mV compared with 150 mV for EtMeO(5)[ZnTrNPc]$_2$ (Tables I and II).[8g] The reduction couples of Ant[ZnTrNPc]$_2$ in DCB look much more irreversible than those in DMF, and spectroelectrochemistry (vide infra) could not be used because of species instability. Probably, the first two reduction couples involve the stepwise reduction of two phthalocyanine rings, but the data are not of sufficient quality to warrant detailed discussion. Nap[ZnTrNPc]$_2$ behaves essentially similar to Ant[ZnTrNPc]$_2$.

The cyclic and differential voltammetric behavior of Nap[CuTrNPc]$_2$ in comparison to CuTNPc is similar to that of Nap[ZnTrNPc]$_2$ or Ant[ZnTrNPc]$_2$ to ZnTNPc in DCB. However, low solubility in DMF hindered determination of some of the redox couples even by DPV. In DCB, Nap[CuTrNPc]$_2$ exhibited two quasi-reversible and one irreversible oxidation and two quasi-reversible reductions (Table I). An additional less intense peak appeared between the first and second reductions, in both solvents. Compared with Nap[ZnTrNPc]$_2$, the potential

(24) The standard oxidation state of the phthalocyanine anion is represented by Pc(-2). Thus the first oxidized and first reduced species will be represented by Pc(-1) and Pc(-3), respectively: Myers, J. F.; Rayner, J. W.; Lever, A. B. P. *Inorg. Chem.* **1975**, *14*, 461.
(25) Walker, F. A. *J. Am. Chem. Soc.* **1973**, *95*, 1150, 1154. Stynes, D. V.; Stynes, H. C.; James, B. R.; Ibers, J. A. *J. Am. Chem. Soc.* **1973**, *95*, 1796. James, B. R. *The Porphyrins*; Vol. V, Dolphin, D. Ed.; Academic Press: New York, 1978; Vol. V, pp 258-277.
(26) Minor, P. C. Ph.D. Thesis, York University, 1983.

Table II. Comproportionation Data

	couple[a]	solvent[b]	E/V[c]	K_c[d]	K_d[e]	ΔG/kJ mol^{-1}
Ant[CoTrNPc]$_2$	I	DCB	0.17	8.4×10^2	1.2×10^{-3}	−17
	II	DCB	0.48	1.8×10^8	5.6×10^{-9}	−47
	III	DMF	0.23	9.0×10^3	1.1×10^{-4}	−23
	II	DMF	0.30	1.4×10^5	7.0×10^{-6}	−29.5
Nap[CoTrNPc]$_2$	I	DCB	0.14	2.8×10^2	2.5×10^{-3}	−14
	II	DCB	0.39	4.0×10^6	2.5×10^{-7}	−38
	III	DMF	0.24	1.3×10^4	7.5×10^{-5}	−24
	II	DMF	0.22	6.1×10^3	1.65×10^{-4}	−22
EtMeO(5)(ZnPc)$_2$[f]	I	DCB	0.08	2.4×10^1	4.2×10^{-2}	−8
	I	DMF	0.15	3.8×10^2	2.6×10^{-3}	−15
(ZnTrNPc)$_4$[f]	I	DCB	0.11	7.8×10^1	1.3×10^{-2}	−11
	I	DMF	0.15	3.8×10^2	2.6×10^{-3}	−15
Ant[ZnTrNPc]$_2$	I	DCB	0.21	4.1×10^3	2.45×10^{-4}	−21
	I	DMF	0.21	4.1×10^3	2.45×10^{-4}	−21
Nap[ZnTrNPc]$_2$	I	DCB	0.21	4.1×10^3	2.45×10^{-4}	−21
	I	DMF	0.18	1.2×10^3	8.0×10^{-4}	−18
Nap[CuTrNPc]$_2$	I	DCB	0.20	2.7×10^3	3.6×10^{-4}	−20
(−1)(ZnPc)$_2$[g]	I	DCB	0.26	2.95×10^4	3.4×10^{-5}	−25
	I	DMF	0.22	6.1×10^3	1.65×10^{-4}	−22
RSiPc–O–PcSiR[h]	I	CH_2Cl_2	0.49	2.7×10^8	3.7×10^{-9}	−49
	II	CH_2Cl_2	0.40	7.6×10^6	1.3×10^{-7}	−40

[a] Couple I: $[MPc(-1)]_2 + [MPc(-2)]_2 \rightarrow 2[MPc(-1)MPc(-2)]$. Couple II: $[Co^{I}Pc(-2)]_2 + [Co^{II}Pc(-2)]_2 \rightarrow 2[Co^{I}Pc(-2)Co^{II}Pc(-2)]$. Couple III: $[Co^{II}Pc(-2)]_2 + [Co^{III}Pc(-2)]_2 \rightarrow 2[Co^{II}Pc(-2)Co^{III}Pc(-2)]$. For the cobalt complexes, data refer to the syn isomer. [b] Solvent DMF = dimethylformamide, DCB = *o*-dichlorobenzene. [c] Mixed-valence splitting energy. [d] Comproportionation constant. [e] Disproportionation constant, $1/K_c$. [f] Reference 8g. [g] Reference 34d. [h] R = n-C_6H_{13}.[10]

difference (1.65 V) between the first oxidation and reduction couples is larger by 0.24 V, while that (0.31 V) between the first and second reductions is smaller by 0.11 V. Possibly the two reduction steps are stepwise one-electron-reduction processes via a mixed-valence reduction species, but solubility problems prevent their elucidation. Figure 4A shows a stick diagram comparison of the relevant mononuclear and binuclear species couples.

(b) Cobalt Derivatives. Voltammograms of the cobalt complexes differ from those of the zinc and copper complexes in showing redox couples due to metal oxidation and reduction. Within the limit of solvent breakdown, in DCB (Figure 5), CoTNPc shows five redox couples, which have been previously assigned[8c] (as indicated in curve A). Nap[CoTrNPc]$_2$ and Ant[CoTrNPc]$_2$ displayed a pair of overlapping couples around 0 V, whose total charge corresponds to two electrons, per binuclear molecule (curves B and C). These couples are assigned to phthalocyanine ring oxidation, based upon spectroelectrochemical data (next section).

The position of this composite couple is approximately the same as that of the first phthalocyanine ring oxidation in Nap[CuTrNPc]$_2$, Nap[ZnTrNPc]$_2$, and Ant[ZnTrNPc]$_2$, the splitting of the two component bands being a little smaller; moreover, the DPV peak to the positive side appears to be larger than the other. The reduction corresponding to the Co(II)/Co(I) couple of CoTNPc, in DCB, shows at least two couples, the more positive DPV wave again being larger in appearance than the other. However since the second reduction step shows some irreversibility (most clearly seen in the cyclic voltammograms), the relative currents in the DP voltammograms may not indicate simple concentration ratios.

Variations in relative DPV heights may also reflect different kinetic parameters for the redox processes involving the syn and anti isomers. The Co(II)/Co(I) splitting in the syn isomer should be somewhat greater than that of the anti isomer. Since the forward and reverse DPVs shown in Figures 5 and 6 are essentially the same, it is possible that the electrochemical data may reflect a larger relative concentration of the syn rather than the anti isomer in the binuclear metal complexes under consideration. The anti isomer, even though involving longer cobalt–cobalt distances than the syn isomer, is expected to show some mixed-valence splitting since it differs from the earlier studied clamshell binuclear species,[8c] in being inflexible (see below). In the zinc species discussed above, the contributions from the two isomers are not distinguished, but these also show greater current in the more positive component of the split waves. Note that these variations in current for components of a given couple do not occur in the

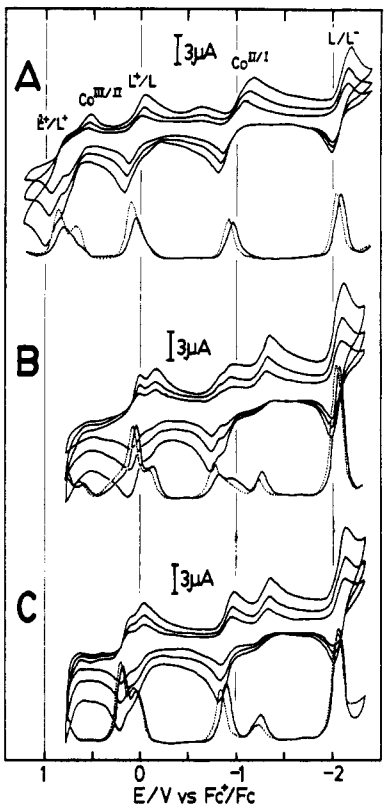

Figure 5. Cyclic and differential-pulse (DP) voltammograms of (A) CoTNPc, (B) Ant[CoTrNPc]$_2$, and (C) Nap[CoTrNPc]$_2$ in DCB at a Pt-disk working electrode. Scan rates/mV s^{-1} = 50, 100, and 200 for cyclic voltammetry and 5 for DPV voltammetry. In DPV diagrams, solid lines indicate cathodic scan and dotted lines indicate anodic scan. [CoTNPc]/M = 6×10^{-4}, [Ant[CoTrNPc]$_2$]/M = 3×10^{-4}, [Nap[CoTrNPc]$_2$]/M = 3.6×10^{-4}, and [TBAP]/M = 0.3. Assignments of redox couples are shown for CoTNPc from the literature.[8c]

EtMeO(5)[ZnTrNPc]$_2$ and zinc tetramer redox processes.[8g]

The splitting of the two bands is ca. 480 mV for Ant[CoTrNPc]$_2$ and 390 mV for Nap[CoTrNPc]$_2$ in DCB, about twice as large as the splitting of the phthalocyanine ring oxidation couples (Table II and III). Although not clear in the case of Nap[CoTrNPc]$_2$, another small but explicit redox couple is

Table III. Electrochemical Data for Mononuclear and Binuclear Cobalt Derivatives

couple	DCB solution		DMF solution	
	$E_{1/2}$/V[a]	ΔE_p/mV[b]	$E_{1/2}$/V[a]	ΔE_p/mV[b]
	CoTNPc System			
$Co^{III}Pc(0)/Co^{III}Pc(-1)$	0.87	140		
$Co^{III}Pc(-1)/Co^{II}Pc(-1)$	0.59	190		
$Co^{III}Pc(-1)/Co^{III}Pc(-2)$	...	...	0.38	80
$Co^{II}Pc(-1)/Co^{II}Pc(-2)$	0.03	125		
$Co^{III}Pc(-2)/Co^{II}Pc(-2)$	...	...	−0.02	75
$Co^{II}Pc(-2)/Co^{I}Pc(-2)$	−0.91	210	−0.85	120
$Co^{I}Pc(-2)/Co^{I}Pc(-3)$	−2.07	145	−1.99	85
	Ant[CoTrNPc]$_2$ System			
$[Co^{III}Pc(-2)]_2/[Co^{III}Pc(-2)Co^{II}Pc(-2)]$	...	...	0.22	50
$[Co^{II}Pc(-1)]_2/[Co^{II}Pc(-1)Co^{II}Pc(-2)]$	0.06	80	...	...
$[Co^{III}Pc(-2)Co^{II}Pc(-2)]/[Co^{II}Pc(-2)]_2$	...	...	−0.01	70
$[Co^{II}Pc(-1)Co^{II}Pc(-2)]/[Co^{II}Pc(-2)]_2$	−0.11	40	...	...
$[Co^{II}Pc(-2)]_2/[Co^{II}Pc(-2)Co^{I}Pc(-2)]$	−0.78	55	−0.73	90
	−0.91	30		
$[Co^{I}Pc(-2)Co^{II}Pc(-2)]/[Co^{I}Pc(-2)]_2$	−1.26[c,d]	110	−1.03[c,d]	90
$[Co^{I}Pc(-2)]_2/[Co^{I}Pc(-3)]_2$	−2.07	115	−1.90	110
	Nap[CoTrNPc]$_2$ System			
$[Co^{III}Pc(-1)Co^{III}Pc(-2)]/[Co^{III}Pc(-2)]_2$			0.41[d]	
$[Co^{III}Pc(-2)]_2/[Co^{III}Pc(-2)Co^{II}Pc(-2)]$	...	...	0.29	70
$Co^{II}Pc(-1)]_2/[Co^{II}Pc(-1)Co^{II}Pc(-2)]$	0.14	60	...	...
$[Co^{III}Pc(-2)Co^{II}Pc(-2)]/[Co^{II}Pc(-2)]_2$	...	...	0.05	60
$[Co^{II}Pc(-1)Co^{II}Pc(-2)]/[Co^{II}Pc(-2)]_2$	0.00	70	...	...
$[Co^{II}Pc(-2)]_2/[Co^{II}Pc(-2)Co^{I}Pc(-2)]$	−0.90	90	−0.87	90
$[Co^{I}Pc(-2)Co^{II}Pc(-2)]/[Co^{I}Pc(-2)]_2$	−1.29[c,d]	100	−1.09[c,d]	150
$[Co^{I}Pc(-2)]_2/[Co^{I}Pc(-3)]_2$	−2.08	110	−1.97	100

[a] Potentials are reported with respect to the ferrocenium/ferrocene couple. $E_{1/2}$ values were measured by cyclic voltammetry at 200, 100, 50, and 20 mV/s. Average data $E = (E_{pa} + E_{pc})/2$ are reported. Data in parentheses are estimated from overlapping waves. Three dots indicate that the specific redox couple is not permissible in that solvent. [b] Values of $\Delta E_p = (E_{pa} - E_{pc})$ are given at a potential sweep rate of 50 mV/s, except for those of Nap[CoTrNPc]$_2$ in DMF (20 mV/s). [c] Irreversible. [d] Reported value of $E_{1/2}$ was obtained by differential-pulse voltammetry.

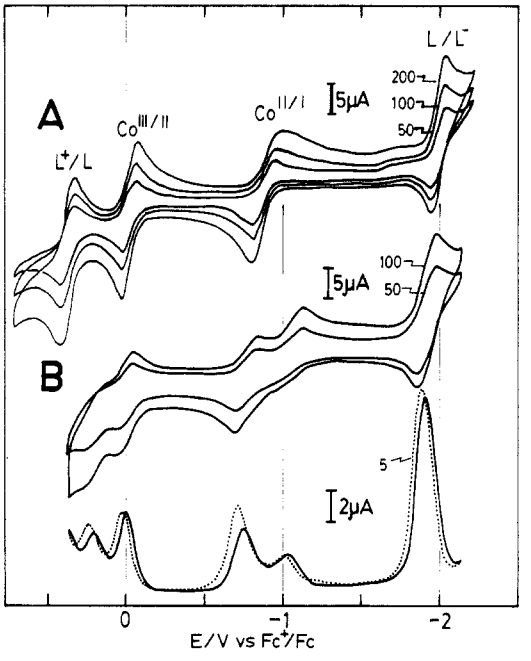

Figure 6. Cyclic and DPV voltammograms of (A) CoTNPc and (B) Ant[CoTrNPC]$_2$ in DMF at a Pt-disk working electrode. Numbers indicate scan rates in mV s^{-1}. In the DPV diagrams, the solid line and dotted line, respectively, indicate cathodic and anodic scans. [CoTNPc]/M = ca. 7.1 × 10^{-4}, [Ant[CoTrNPc]$_2$]/M = ca. 3.8 × 10^{-4}, and [TBAP]/M = 0.3. Assignments of redox couples are shown for CoTNPc from the literature.[8c]

discerned for Ant[CoTrNPc]$_2$ at ca. −0.9 V vs Fc$^+$/Fc (curve B); this may be the first reduction couple for the anti isomer. We return to this discussion below (spectroelectrochemistry).

In DMF,[8c] CoTNPc shows Co(II)/Co(I) and Co(III)/Co(II) couples before the reduction and oxidation respectively of the ligand (see also Figure 6A). The corresponding couples in Ant[CoTrNPc]$_2$ and Nap[CoTrNPc]$_2$ are split, and the area of each peak in the DPV voltammogram (see Figure 6B for Ant-[CoTrNPc]$_2$) roughly corresponds to one electron per binuclear molecule (Table III).

In both DCB and DMF, the first reduction of the two phthalocyanine rings occurs simultaneously at the same potential around −2 V. Compared with the first ring reduction of dizinc and dicopper derivatives, the potential is roughly 500 mV more negative, a consequence of the central Co(I) metal ion, compared with central Zn(II) and Cu(II) metal ions in the former species.[8f] This $Co^{I}Pc(-2)/Co^{I}Pc(-3)$ anion-radical reduction wave is unsplit and occurs at essentially the same potential in the mononuclear CoTNPc and, evidently, both the syn and anti isomers of the Nap and Ant binuclear species. This must be a net two-electron-reduction process (per binuclear molecule) in the latter species.

(iii) Comproportionation Constants. In order to obtain information about the stability of mixed-valence species, comproportionation constants (K_c at 20 °C) of the mixed-valence formation reactions were calculated, by using eq 1 (Table II), where ΔE is

$$[MPc(-1)]_2 + [MPc(-2)]_2 \rightarrow 2[MPc(-1)MPc(-2)] \quad (I)$$

$$[Co^{I}Pc(-2)]_2 + [Co^{II}Pc(-2)]_2 \rightarrow 2[Co^{I}Pc(-2)Co^{II}Pc(-2)] \quad (II)$$

$$[Co^{II}Pc(-2)]_2 + [Co^{III}Pc(-2)]_2 \rightarrow 2[Co^{II}Pc(-2)Co^{III}Pc(-2)] \quad (III)$$

$$\Delta E = (RT/F) \ln K_c \quad (1)$$

the splitting energy for the relevant split redox couple. The K_c values lie approximately in the 1 × 10^3–3 × 10^8 range (ΔG = ca. −17 to −49 kJ mol^{-1}), indicative of significant delocalization in many of the complexes.[27] Table II contains a comparison of literature data for related processes (see section viii below for further comment).

(27) (a) Gagne, R. R.; Spiro, C. L.; Smith, T. J.; Haman, C. A.; Thies, W. R.; Shiemke, A. K. *J. Am. Chem. Soc.* **1981**, *103*, 4073. (b) Sutton, J. E.; Taube, H. *Inorg. Chem.* **1981**, *20*, 319. (c) Suzuki, M.; Uehara, A.; Oshio, H.; Yanaga, M.; Kida, S.; Sato, K. *Bull. Chem. Soc. Jpn.* **1987**, *60*, 3547.

Table IV. Electronic Spectroscopic Data[a]

complex	solvent	spectroscopic data λ/nm ($10^{-4}\epsilon/M^{-1}$ cm^{-1})				
$Co^{II}TNPc$	DMF	326 (8.51)	380 sh		606 (3.89)	668 (11.0)
	DCB	330 (4.07)	380 (1.38)		612 (2.57)	678 (7.24)
$Ant[Co^{II}TrNPc]_2$	DMF	305 (11.77)	327 sh		630 (8.89)	659 (8.71)
	DCB	335 sh	393 sh		640 (7.08)	672 (7.41)
$[Co^{II}Co^{I}]$	DCB	328 sh	432 sh	480 sh		660 (8.12)
$[Co^{I}Co^{I}]$	DCB		436 sh	472 (7.23)	648 (3.84)	710 (8.93)
$[Co^{II}Pc(-1)]_2$	DCB	363 (4.72)	494 (2.52)			672 (6.36)
$Nap[Co^{II}TrNPc]_2$	DMF	307 (10.5)			626 (8.07)	675 sh (6.89)
	DCB	322 sh	388 sh		634 (7.42)	671 (7.01)
$[Co^{II}Co^{I}]$	DCB	312 (11.0)	440 br (2.5)	480 sh		650 (7.5)
$[Co^{I}Co^{I}]$	DCB	308 (7.8)	428 sh	465 (6.5)	642 (4.5)	703 (7.8)
$[Co^{II}Pc(-1)]_2$	DCB	324 (7.3)	400 sh	572 br (4.0)		680 (4.3)
ZnTNPc	DCB	356 (8.6)			614 (4.0)	680 (18.8)
$Nap[ZnTrNPc]_2$	DMF	281 (7.16)	343 (13.01)		635 (11.6)	672 (11.45)
	DCB	340 (12.6)			641 (11.7)	679 (10.9)
$Ant[ZnTrNPc]_2$	DMF	280 (5.09)	342 (7.02)		638 (6.34)	672 (7.79)
	DCB	340 (6.08)			643 (5.24)	678 (5.43)
$Nap[Cu^{II}TrNPc]_2$	DMF	277 (5.26)	336 (5)		634 (6.11)	673 (5.23)
	DCB	338 (5.41)			639 (5.81)	678 (5.14)

[a] Data for unelectrolyzed species were collected by using solutions (6–8) × 10^{-6} M in a 10-mm cell at 20 °C, while those of electrochemically generated species were obtained by using solutions ca. 10^{-3}–10^{-4} M in 1-mm or 0.045-mm OTTLE cells in the presence of ca. 0.3 M TBAP (electrolyte). Note that the presence of electrolyte can influence the degree of aggregation, as can concentration. Thus spectra obtained in the presence and in the absence of electrolyte and at different concentrations may not be exactly the same.

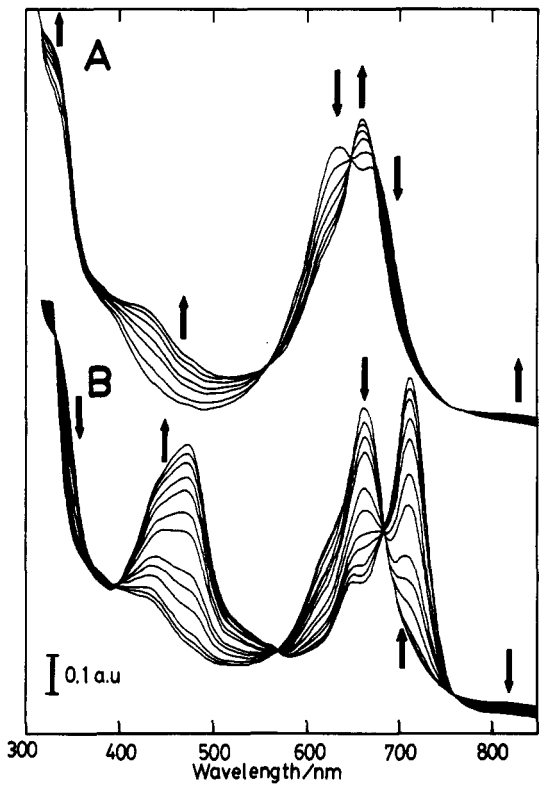

Figure 7. Development of the electronic spectra of $Ant[CoTrNPc]_2$ in DCB with time, showing the formation of (A) the mixed-valence $[Co^{II}TrNPcCo^{I}TrNPc]^-$ species and (B) the doubly reduced $[Co^{I}TrNPcCo^{I}TrNPc]^{2-}$ species obtained by reduction at potentials between −0.8 and −1.2 V, and −1.3 and −1.6 V, respectively. $[Ant[CoTrNPc]_2]/M = 1.17 \times 10^{-4}$. [TBAP]/M = 0.3. Path length/mm = 0.45.

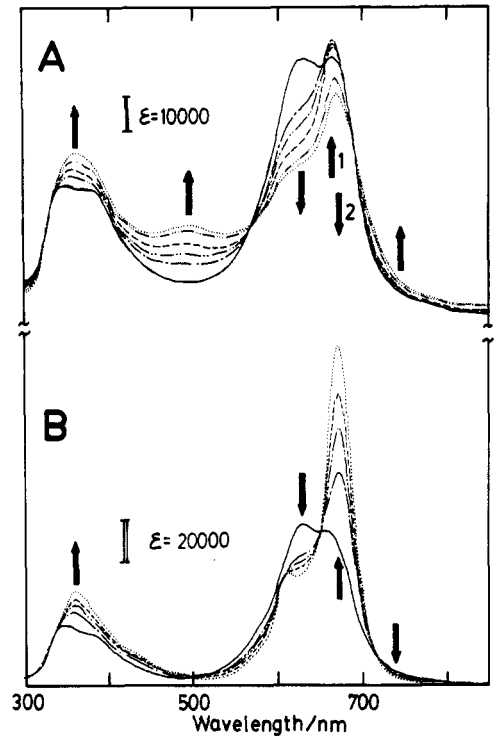

Figure 8. Development of the electronic spectra of $Ant[CoTrNPc]_2$ in (A) DCB or in (B) DMF, showing the formation of (A) $Ant[Co^{II}TrNPc(-2)Co^{II}TrNPc(-1)]^+$ and then $Ant[Co^{II}TrNPc(-1)]_2^{2+}$ species, and (B) the doubly oxidized $Ant[Co^{III}TrNPc(-2)]_2^{2+}$ species obtained by oxidation at potentials between −0.5 and +0.6 V. Path length/mm = 0.45. $[Ant[CoTrNPc]_2]/M = 1.27 \times 10^{-4}$ in DCB and 2.05×10^{-4} in DMF. [TBAP]/M = 0.3.

(iv) Electronic Spectra. The rigid geometry of the naphthalene or anthracene bridge induces important changes in these cofacial metal derivatives, compared with mononuclear phthalocyanines.[8c] The divalent metal $M^{II}Pc(-2)$ species all show a doubled Q-band (Table IV, Figures 7 and 8, and Figure 1a of ref 8a) indicative of exciton interaction between the halves of the molecule.[28,29] The situation is complicated by the presence of both the syn and anti isomers but the higher energy component can securely be assigned to the allowed Q-band, exciton split, component of the syn isomer. The lower energy absorption then arises from overlap of anti isomer absorption and weaker "forbidden" syn isomer absorption.

Assuming no ground-state interaction between the π levels of the phthalocyanine rings, the exciton splittings in the syn isomer may be estimated as twice the difference between the higher energy

(28) Kasha, M.; Rawls, H. R.; Et-Bayoumi, M. A. *Pure Appl. Chem.* **1965**, *11*, 371.

(29) Dodsworth, E. S.; Lever, A. B. P.; Seymour, P.; Leznoff, C. C. *J. Phys. Chem.* **1985**, *89*, 5698.

Table V. Exciton Splitting, Q-Transition Envelope, π-Orbital Shift, and Ring-Oxidation Splitting

complex[a]	solvent	exciton splitting/cm^{-1} uncor[g]	exciton splitting/cm^{-1} cor[h]	half-bandwidth/cm^{-1} [b]	rel ratio[c]	Q-band max/cm^{-1} [d]	π shift (y)/V[e]	ΔE/V[f]
Nap[ZnTrNPc]$_2$	DMF	1890	2860	900	1.15	15750	0.06	0.18
	DCB	1650	3580	2300	1.15	15650	0.12	0.21
Ant[ZnTrNPc]$_2$	DMF	1690	3300	2025	0.82	15670	0.10	0.21
	DCB	1700	3470	2480	0.93	15550	0.11	0.21
EtMeO(5)[ZnTrNPc]$_2$	DCB	2340	3310			15900	0.06	0.08
ZnTNPc	DCB			650[i]				
Nap[CoTrNPc]$_2$	DMF	2000			1.17	15970		
	DCB	2250	2730	2700	1.30	15900	0.03	0.14
Ant[CoTrNPc]$_2$	DMF	1800		2400	1.01	15870		
	DCB	1750	4000	2520	0.98	15625	0.14	0.17
Nap[CuTrNPc]$_2$	DMF	2020		2520	1.4			0.27
	DCB	1540		2320	1.35			0.20
EtMeO(5)[CoTrNPc]$_2$	DCB	2450	2450			15970	0.0	0.0

[a] All complexs contain the divalent metal ion. [b] Half-bandwidth of composite Q-band envelope measured at half the intensity of the strongest component. [c] Relative ratio of the peak molar intensities of the shorter to longer wavelength transitions. (N.B.—this will vary slightly as a function of concentration and added electrolyte). [d] Higher energy Q-band maximum. [e] Variable y (see text) is the difference between first ring-oxidation potential of mononuclear MTNPc (M = Co or Zn), and the lower component of the first ring-oxidation potential of the binuclear species. [f] Ring-oxidation splitting. [g] "Uncorrected" Q-band exciton splitting, measured according to the method in the text. [h] "Corrected" exciton coupling obtained from sum of the "uncorrected" value plus $2y$ (expressed in cm^{-1}) by multiplying the volt value by 8065) and rounded off to the nearest 10 cm^{-1}). [i] Half-bandwidth of the Q-band in monomeric ZnTNPc from data in ref 8g.

component in the Q-band absorption of the binuclear species, and the Q-band observed in the mononuclear MTNPc control molecules[8c,8g] in the solvent concerned (Table IV). In this fashion the so-called "uncorrected" data in Table V are derived. Exciton coupling is also estimated, qualitatively, from the ratio of the peak intensities of the higher energy Q component to that of the lower energy. The greater the degree of coupling between the halves of the molecule, the greater will be the intensity of the higher energy component; such data are also reported in Table V.

However the existence of mixed-valence ring-oxidation species is a direct indication of a ground-state interaction between the phthalocyanine π levels. Indeed the extent of electrochemical splitting, ΔE, of the pair of oxidation levels is *inversely* proportional to the "uncorrected" exciton energies (cf. Tables II and V). This is contrary to the intuitive expectation that the greater the ground-state interaction, the greater the degree of exciton coupling.

A qualitative molecular orbital description might be written as in Figure 9. To the extent that the ground-state π levels interact as in Figure 9, the Q-band transition will be red-shifted, nominally by the energy y (in Figure 9), relative to the mononuclear species. The quantity y is related to ΔE (for ring oxidation) and it is relevant that the higher energy Q-band component does shift to *lower* energy with increasing ΔE. This provides evidence that this sample qualitative model, which has also been used to describe the properties of silicon phthalocyanine dimers and trimers,[10] has merit and explains the apparent inverse dependence mentioned immediately above.

The quantity y may be approximated as the difference in energy between the first oxidation potential of the control mononuclear MTNPc species and the more negative of the split components of the oxidation of the binuclear species. The values of y are also shown in Table V and do generally increase with increasing (ring-oxidation) splitting energy ΔE. The "corrected" exciton splitting is then approximately equal to the "uncorrected" value plus $2y$. These data are also reported in Table V.

Although the "corrected" exciton coupling energies are subject to some uncertainty, an increase in exciton splitting does parallel an increase in electrochemical (ring oxidation) splitting, ΔE, of the ground state for these and related binuclear cobalt and zinc species (Tables III and V).

Q-Band half-bandwidths are also listed in Tables II and V. They are a complex function since the Q-band, normally of half-bandwidth around 300–800 cm^{-1}, will broaden as a consequence of some exchange coupling. However, in the limit of coupling between two phthalocyanine rings where the binuclear species is strictly of D_{4h} symmetry, the bandwidth becomes narrower due to loss of the lower energy transition, which becomes forbidden.[29] For example, the highly cofacial crown ether

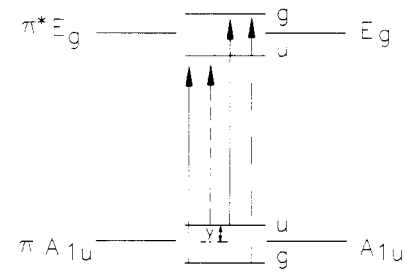

Figure 9. Molecular orbital description of the interaction between the π and π^* levels of a pair of interacting cofacial phthalocyanine rings. The arrows indicate allowed transitions, while the hatched lines indicate forbidden transitions in D_{4h} symmetry. The allowed transitions are of approximately the same energy and correspond with the observed high-energy component of the Q-band in the binuclear species. The energy y corresponds approximately with the difference in first oxidation potential of the mononuclear and binuclear species. In this model, the u → u transition becoming slightly allowed in reduced-symmetry acentric species provides the long wavelength tail of the Q-band absorption.

phthalocyanine binuclear species have half-bandwidths on the order of 700–1000 cm^{-1}.[21] The rather larger values reported here in Table V reflect the presence of the anti isomer, and the relatively low symmetry of the cofacial syn isomer. The narrowness of the Q-band for the Nap[ZnTrNPc]$_2$ species in DMF is, however, noteworthy.

Comparisons of the band envelopes of the anthracene and naphthalene cobalt(II) species with those of the clamshell species (Figure 5 of ref 8c) show that the latter have slightly greater absorption in the long wavelength tail, even though the half-bandwidths (ca. 2700–2800 cm^{-1}) are essentially the same. The lack of a long wavelength tail in the Q-band region of the naphthalene and anthracene species suggests that they conform more closely to D_{4h} symmetry than do the flexible clamshell species.

(v) Spectroelectrochemistry. To assign the redox couples and to observe the interaction between the halves of the molecules, as a function of oxidation state, spectroelectrochemical experiments were performed for Ant[CoTrNPc]$_2$ and Nap[CoTrNPc]$_2$ in optically transparent thin-layer electrode (OTTLE) cells. Data for the naphthalene species have been previously briefly described (Figure 1 of ref 8a). Figure 7 shows the absorption spectra of Ant[CoTrNPc]$_2$ in DCB. In a manner similar to reduction of the Nap[CoTrNPc]$_2$ species,[8a] reduction across the first couple results in the spectroscopic changes shown in A, with isosbestic points occurring at 562, 648, and 765 nm and a change of color from blue to green.

In common with $Co^{I}Pc$ species, a new absorption band appears in the region of 400–500 nm, associated with metal-to-ligand charge transfer (MLCT) from cobalt(I) to the phthalocyanine ring;[30] there is also an increase in intensity in the Soret region. The Q-band spectrum of this green solution and that of the corresponding $Nap[CoTrNPc]_2$ reduced species are unlike any seen previously for reduced cobalt phthalocyanines,[19,30] having a strong Q-band at ca. 660 nm instead of the usual band at 710 nm. This is similar, however, to the mixed-valence flexible clamshell $EtMeO(5)[ZnPc(-2)ZnPc(-1)]^{+}$ species described earlier.[8g]

The second reduction between −1.3 and −1.8 V (Figure 7B) gives a yellow solution, with isosbestic points at 329, 395, 570, 683, and 762 nm. The final spectrum is very similar to that of the mononuclear $Co^{I}TNPc$ species;[8c] thus, both cobalt atoms have been reduced to Co(I). The reduced ($Co^{I}Co^{I}$) species is fully reversible to the starting material by oxidation positive of the first reduction couple on the spectroelectrochemical time scale (minutes) even though the second reduction step is irreversible.

Nernstian plots of the spectroelectrochemical data over each of the reduction processes give slopes of 55 and 48 mV (for the first and second reduction, respectively, of $Nap[CoTrNPc]_2$ in DCB), and intercepts of −0.29 and −0.64 V vs AgCl/Ag, respectively; thus, each step involves a one-electron transfer, and the product of the first reduction must be a mixed-valence species of mainly $[Co^{II}TrNPcCo^{I}TrNPc]^{-}$ character. Taking the Fc^{+}/Fc couple to be about 0.59 V vs AgCl/Ag gives intercept values of −0.88 and −1.23 V vs Fc^{+}/Fc, which are close to the values measured by CV (Table III).

For the mixed-valence $[Co^{II}TrNPcCo^{I}TrNPc]^{-}$ species (Figure 7A) the intensity of the MLCT band appears to be only about 20% of that of the fully reduced $[Co^{I}TrNPcCo^{I}TrNPc]^{2-}$ species. This may signify that, at the potential employed to obtain this electronic spectrum, only the syn isomer is reduced fully to $Co^{II}Co^{I}$ while the anti isomer, which would be reduced at a somewhat more negative potential, is only partially reduced to $Co^{II}Co^{I}$. Given the overlapping nature of the Q-band spectra of the $Co^{II}Co^{II}$ and $Co^{II}Co^{I}$ species, the spectrum shown in Figure 7A for the mixed-valence species might well contain some unreduced anti species.

The presence of the well-resolved Q-band at 660 nm, rather than 710 nm, indicates some coupling between the formal Co(II) and Co(I) halves of the molecule. A weak absorption band of the first reduction product in the region of 800–900 nm (Figure 7A) may be an intervalance band. $Nap[CoTrNPc]_2$ also shows similar spectroscopic changes in the corresponding processes.[8a] The positions of the Q-band peaks of the first- and second-reduction products, however, are shifted by about 10 nm to shorter wavelength compared with $Ant[CoTrNPc]_2$.

The similarity in the final spectrum of the $[Co^{I}TrNPcCo^{I}TrNPC]^{2-}$ species to that of mononuclear $[Co^{I}TNPc]^{-}$ requires that there is little interaction between the halves of the binuclear molecule in the $[Co^{I}TrNPcCo^{I}TrNPc]^{2-}$ species. Each half will carry a net negative charge and this may force them slightly further apart than in the $[Co^{II}TrNPcCo^{II}TrNPc]$ or $[Co^{II}TrNPcCo^{I}TrNPc]^{-}$ species. Evidently both the syn and anti forms of the $[Co^{I}TrNPc(-2)$-$Co^{I}TrNPc(-2)]^{2-}$ species must have very similar spectra. Similar behavior is observed in DMF solution.

Figure 8A demonstrates spectroscopic changes of $Ant[CoTrNPc]_2$ in DCB observed during stepwise oxidation. As seen in Figure 5B, the first oxidation couples are composed of a superimposition of two couples. Changes in Figure 8A also contain two processes. In the oxidation between −0.4 and −0.1 V, the absorbance of a peak at 635 nm decreases but that at 670 nm increases, while in the second oxidation at potentials higher than 0 V, the absorbance in the whole Q-band region decreases. During these oxidations, the absorbance at ca. 340–570 nm increases. In the oxidation of phthalocyanines, the increase of absorbance in the region between the Soret band and the Q-band is an indication of phthalocyanine ring oxidations;[8c,g,31,32] therefore, the first oxidation of $Ant[CoTrNPc]_2$ in DCB forms the cobalt(II) phthalocyanine cation-radical species.

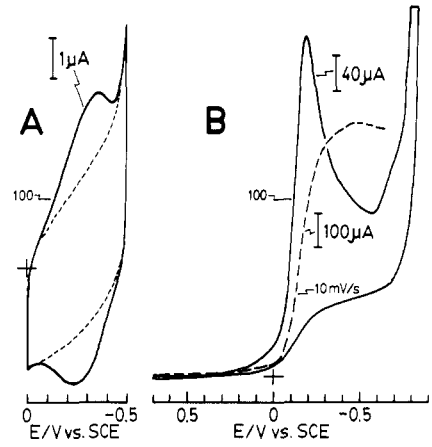

Figure 10. Cyclic voltammograms (solid lines) and RRDE response (broken line) at $Nap[CoTrNPc]_2$ adsorbed on OPG electrode in the (A) absence and (B) presence of oxygen in 0.05 M H_2SO_4. In part A, the dotted line indicates response at a bare OPG electrode. Numbers in the figure indicate scan rate in mV s^{-1}.

Figure 8B shows the spectroscopic changes of $Ant[CoTrNPc]_2$ in DMF observed during the first oxidation. As the potential is increased through the region of the two oxidation waves, a peak at 630 nm decreases but that at 660 nm develops into an intense peak at 673 nm. During this process, no new peak appears between the Soret band and the Q-band. This behavior is typical for the oxidation of cobalt(II) to cobalt(III) phthalocyanine.[8c,d,30d,e,33]

The spectroscopic development in Figure 8B corresponds to the process from the $[Co^{II}TrNPcCo^{II}TrNPc]$ to the fully oxidized $Ant[Co^{III}TrNPc]_2^{2+}$ species with no distinct intermediate spectrum attributable to a mixed-valence $[Co^{III}TrNPcCo^{II}TrNPc]^{+}$ species being observed. Such a species must certainly exist. However the Q-band energy maxima for $Co^{II}TNPc$ and $Co^{III}TNPc$ are essentially identical.[8c] Thus, in the absence of a strong perturbing interaction between the halves of the mixed-valence species, its spectroscopic signature will be difficult to discern. Indeed the inability to see this intermediate leads one to exclude a strong spectroscopic perturbation for this mixed-valence species.

(vi) Immobilization of Nap- and Ant$[CoTrNPc]_2$ on OPG. Argon Data. Figure 10 shows the cyclic voltammograms at $Nap[CoTrNPc]_2$ adsorbed on OPG in a deaerated 0.05 M H_2SO_4 solution. A redox couple with equal reduction and oxidation current is seen at ca. −0.28 V vs SCE. The potential of this couple shifts with changing pH of the solution as demonstrated in Figure 11, shifting negatively with increasing pH between pH 1 and 7 with a slope of −60 to −70 mV/pH unit; above ca. pH 9, it becomes essentially pH independent. Similar behavior has been found in several cobalt phthalocyanine systems,[34] and the relevant couple

(30) (a) Nevin, W. A.; Liu, W.; Melnik, M.; Lever, A. B. P. *J. Electroanal. Chem. Interfacial Electrochem.* **1986**, *213*, 217. (b) Rollman, L. D.; Iwamoto, R. T. *J. Am. Chem. Soc.* **1968**, *90*, 1455. (c) Clack, D. W.; Yandle, J. R. *Inorg. Chem.* **1972**, *11*, 1738. (d) Day, P.; Hill, H. A. O.; Price, M. G. *J. Chem. Soc. A* **1968**, *90*. (e) Stillman, M. J.; Thompson, A. J. *J. Chem. Soc., Faraday Trans. 2* **1974**, *70*, 790. (f) Le Moigne, J.; Even, R. J. *J. Chem. Phys.* **1985**, *82*, 6472. (g) Taube, R. *Z. Chem.* **1966**, *6*, 8. (h) Lever, A. B. P.; Licoccia, S.; Magnell, K.; Minor, P. C.; Ramasawamy, B. S. *ACS Symp. Ser.* **1982**, *No. 201*, 237.

(31) Minor, P. C.; Gouterman, M.; Lever, A. B. P. *Inorg. Chem.* **1985**, *24*, 1894.

(32) (a) Dolphin, D.; James, B. R.; Murray, A. J.; Thornback, J. R. *Can. J. Chem.* **1980**, *58*, 1125. (b) Ferraudi, G.; Oishi, S.; Muraldiharan, S. *J. Phys. Chem.* **1984**, *88*, 5261. (c) Nyokong, T.; Gasyna, Z.; Stillman, M. J. *Inorg. Chim. Acta* **1986**, *112*, 11. (d) Gavrilov, V.; Tomilova, L. G.; Shelepin, I. V.; Luk'yanets, E. A. *Elektrokhimiya* **1979**, *15*, 1058.

(33) Homborg, H.; Kalz, W. *Z. Naturforsch., B: Anorg. Chem., Org. Chem.* **1984**, *39B*, 1490. Kalz, W.; Homborg, H.; Kuppers, H.; Kennedy, B. J.; Murray, K. S. *Z. Naturforsch., B: Anorg. Chem., Org. Chem.* **1984**, *39B*, 1478.

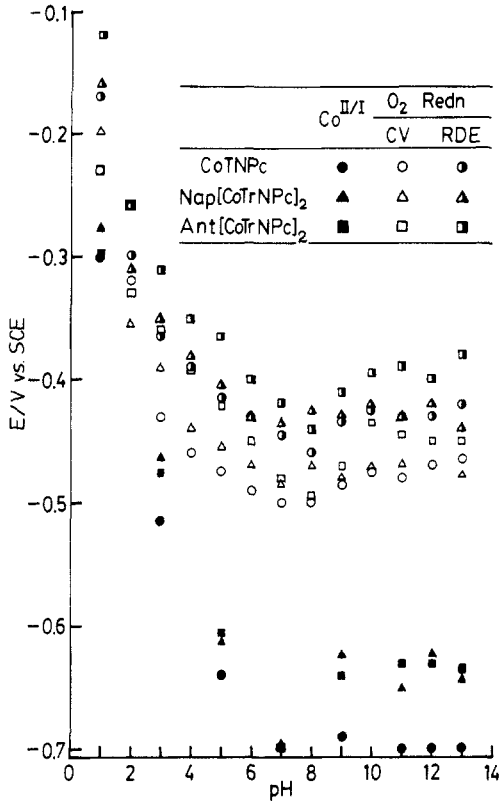

Figure 11. pH dependence of the Co(II)/Co(I) redox potential of CoTNPc, Nap[CoTrNPc]$_2$, and Ant[CoTrNPc]$_2$ adsorbed onto OPG, and that of the O_2 reduction potential at these phthalocyanine-adsorbed electrodes. In oxygen reduction, peak potentials (CV method) or half-wave potentials (RRDE method) are plotted.

is ascribed to that of Co(II)/Co(I).

Assuming the wave corresponds to a Faradaic change in the charge of the adsorbed species by nF, and the system behaves ideally, the ratio of the slope of a plot of peak current vs sweep rate to the charge should be equal to $nF/4RT$, where n is the number of electrons per adsorbed species and the other symbols have their usual meaning.[35] Experimental values give unexpectedly lower values of $(0.5–0.6)F/RT$ compared with those of $(0.8–0.9)F/RT$ for a mononuclear control molecule, CoTNPc.[34a] Such low values have been observed previously for immobilized cofacial porphyrins[4f] and attributed to the presence of inactive material on the surface. In the case of the porphyrin, the surface concentration was derived from consideration of how much material was laid upon the electrode surface. In this case, using the slope analysis, any inactive material will contribute to neither q nor n, and the calculation is therefore unresponsive to the presence of inactive material on the surface, except insofar as this may have kinetic significance. Indeed the simple analysis described here would only be valid for pure Nernstian behavior and fast kinetics.[16] It is possible that the deviation from one electron per cobalt atom is attributable to kinetic interference in the electron transfer. Nevertheless it is interesting that it is the adsorbed binuclear phthalocyanine species, and not the mononuclear species, which give rise to this reduced value of n.

This wave is therefore the first reduction wave to the mixed valence Nap[Co^{II}TrNPcCo^{I}TrNPc]$^-$ species on the surface. The second reduction wave should be seen some 0.2–0.5 V more negative; however, proton reduction to hydrogen is catalyzed by cobalt phthalocyanine[36] and occurs some 0.15–0.20 V more negative than the first wave, thereby obscuring this second wave. Moving to higher pH does not alleviate the problem since proton reduction tracks the pH behavior of this first couple. No advantage was found in switching to stress-annealed pyrolytic graphite as support material. Thus the second reduction wave cannot be identified.

(vii) Electrocatalytic Reduction of Oxygen. When the solution in Figure 10A is saturated with oxygen, the responses shown in Figure 10B are obtained. In cyclic voltammograms, a cathodic peak appears at −0.20 V vs SCE whose current (i_p) is proportional to the concentration of oxygen and the square root of the scan rate, indicating that this i_p is controlled by the diffusion of oxygen. Compared with the Co(II)/Co(I) redox couple of this catalyst, the catalytic O_2 reduction wave appears at a more positive potential at all pHs.

Using standard rotating disk electrode (RDE) methods[34b,35,37,38] two-electron reduction of oxygen to hydrogen peroxide is observed. A rotating ring–disk electrode experiment (not shown) detected hydrogen peroxide at the ring electrode upon reduction of oxygen at the disk electrode. Similar electrochemical behavior is also observed at Ant[CoTrNPc]$_2$-modified electrodes. Thus, in contrast to some cofacial bis(cobalt) porphyrins,[11,12] which catalyze O_2 reduction by a four-electron pathway to water at pH less than 2, Nap- and Ant[CoTrNPc]$_2$ catalyze O_2 reduction only to hydrogen peroxide in the pH range 1–14.

In considering the mechanism of O_2 reduction, it is clear at least that cobalt is participating in the reaction, since the O_2 reduction peak potential tracks the Co(II)/Co(I) redox potential at all pHs; however, the mechanism is unclear. Although the potential difference between the Co(II)/Co(I) couples and O_2 reduction peak is a little over 200 mV in alkaline solution, an EC mechanism is possible if the reaction rate is very fast.[39] The potential difference of 200 mV, for example, corresponds to a reaction rate of ca. 5×10^8 M^{-1} s^{-1}, which is an order of magnitude larger than those for some porphyrin[38,40] and phthalocyanine[19] systems. This problem has been discussed in depth elsewhere, where an alternate mechanism involving binding of oxygen to cobalt(II) phthalocyanine is presented.[34b]

(viii) Concluding Comments. The electrochemical behavior of the cofacial phthalocyanine binuclear molecules in this paper is similar to that of the cofacial porphyrins.[4–7] In these complexes, splitting of both the Co(II)/Co(I) and Co(III)/Co(II) redox couples has been observed and appears a function of the nature of the inter-ring linkage. $Co^{II}Co^{I}$ splitting energies of some 0.25–0.4 V are observed, perhaps a little smaller than the largest observed here. Curiously for the 1,8-anthracene-linked cofacial dicobalt diporphyrin (Ant[CoPor]$_2$),[4a] which has a structure similar to that of Ant[CoTrNPc]$_2$, there is no observable splitting of the Co(II)/Co(I) wave, and no dramatic change in the electronic spectrum. Metallophthalocyanines[41] are more planar than porphyrins[42] and, perhaps because of this property, have a much higher tendency toward cofacial aggregation than porphyrins.[43]

(34) (a) Zecevic, S.; Simic-Glavaski, B.; Yeager, E.; Lever, A. B. P.; Minor, P. C. *J. Electroanal. Chem. Interfacial Electrochem.* **1985**, *196*, 339. (b) Janda, P.; Kobayashi, N.; Auburn, P. R.; Lam, H.; Leznoff, C. C.; Lever, A. B. P. *Can. J. Chem.* **1989**, *67*, 1109.
(35) Zagal, J.; Bindra, P.; Yeager, E. *J. Electroanal. Chem. Interfacial Electrochem.* **1977**, *83*, 207.
(36) Bernstein, P.; Lever, A. B. P. Paper in preparation.
(37) (a) Durand, R. R.; Anson, F. C. *J. Electroanal. Chem. Interfacial Electrochem.* **1982**, *134*, 273. (b) Shigehara, K.; Anson, F. C. *J. Phys. Chem.* **1982**, *86*, 2776.
(38) (a) Forshey, P. A.; Kuwana, T. *Inorg. Chem.* **1981**, *20*, 693; **1983**, *22*, 699. (b) Forshey, P. A.; Kuwana, T.; Kobayashi, N.; Osa, T. *Adv. Chem. Ser.* **1982**, *No. 201*, 601.
(39) (a) Oyama, N.; Oki, N.; Ohno, H.; Ohnuki, Y.; Matsuda, H.; Tsuchida, E. *J. Phys. Chem.* **1983**, *87*, 3642. (b) Andrieux, C. P.; Saveant, J. M. *J. Electroanal. Chem. Interfacial Electrochem.* **1982**, *134*, 163; **1982**, *142*, 1. (c) Andrieux, C. P.; Dumas-Bouchiat, J. M.; Saveant, J. M. *J. Electroanal. Chem. Interfacial Electrochem.* **1982**, *131*, 1.
(40) (a) Kobayashi, N.; Fujihira, M.; Osa, T.; Kuwana, T. *Bull. Chem. Soc. Jpn.* **1980**, *53*, 2195. (b) Kobayashi, N.; Osa, T. *J. Electroanal. Chem. Interfacial Electrochem.* **1983**, *157*, 269. (c) Ozer, P.; Parash, R.; Broitman, F.; Mor, U.; Bettelheim, A. *J. Chem. Soc., Faraday Trans. 1* **1984**, *80*, 1139.
(41) Robertson, J. M.; Woodward, I. *J. Chem. Soc.* **1937**, 219.
(42) (a) Hoard, J. L. In *Porphyrins and Metalloporphyrins*; Smith, K. M., Ed.; Elsevier: Amsterdam, New York, Oxford, England, 1975; Chapter 8. (b) Scheidt, W. R. In *The Porphyrins*; Dolphin, D., Ed.; Academic Press: New York, London, 1978; Vol. III, Chapter 10.
(43) (a) Reference 3 in ref 21. (b) White, W. I. In *The Porphyrins*; Dolphin, D., Ed.; Academic Press: New York, London, 1978; Vol. V, Chapter 7.

The approach of the two phthalocyanine units in one naphthalene or anthracene binuclear species may be closer, therefore, than in the corresponding binuclear porphyrin.

Table II summarizes the splitting energies observed for a range of phthalocyanine species. Although several factors affect the size of K_c,[27a] electrostatic interactions must play an important role. Particularly in the syn form, the two phthalocyanine planes are in close proximity. However the distance between the phthalocyanine units in the 1,8-naphthalene species has been estimated as at least 4.3 Å (section i), compared with the van der Waals contact (3.6 Å) (or shorter in some silicon-bridged phthalocyanine species, 3.3 Å).[9c,10] The mixed-valence splitting energies for oxidation of the silicon phthalocyanine RSiPc-O-PcSiR binuclear species are on the order of 0.4-0.5 V[10] and therefore rather larger than those reported here. This value is indicative of that to be expected at close contact when the rings are well aligned.

The mixed-valence splitting energies for reduction of the silicon binuclear species are about 0.4 V[10] and likely provide an upper limit for sideways interactions of the π clouds in the reduced ring species. This splitting is comparable or less than the $Co^{II}Co^{I}$ splitting data reported here. These larger $Co^{II}Co^{I}$ values are likely a consequence of the interaction between the cobalt d_{z^2} orbitals, which point directly toward one another along the inter-ring axis. While magnetic studies could provide useful information concerning the electronic structures of both the $[Co^{II}TrNPcCo^{II}TrNPc]$ and $[Co^{II}TrNPcCo^{I}TrNPc]^-$ species of complexes, it is premature to attempt such measurements until a means has been found to separate the syn and anti isomers.

Comparison of the "corrected" exciton data (Table V) of these anthracene and naphthalene species with those for the flexible clamshell EtMeO(5) species does show that the former species have greater exciton splitting and this is consistent with the increased electrochemical mixed-valence splitting.

The lack of mixed-valence oxidation products for the cobalt flexible clamshell species may reflect the formation of six-coordinate Co(III) species when a donor solvent or electrolyte anion is present, thus forcing the two rings apart. This may also occur with $Co^{II}Pc(-1)$ species since formation of the Pc(-1) oxidation state will increase the Lewis acidity of the cobalt atom.

Stepwise oxidation of the two rings in a binuclear phthalocyanine species places a positive charge on one ring, which will then attract the electron density on the other ring, favoring formation of a mixed-valence delocalized oxidation species. On the other hand, there is no firm evidence for the formation of mixed-valence anion-radical species in the current series of binuclear complexes, albeit that the DCB electrochemical data are ambiguous in this respect. In this redox level, there is an added electron making one ring negatively charged and causing repulsion of the other ring.

Thus mixed-valence behavior has been established for the following classes of phthalocyanine compounds.

Pc(-1)Pc(-2) is observed with cobalt and in main-group species such as silicon and zinc. Although not fully investigated here, it is likely that mixed-valence Pc(-1)Pc(-2) species containing either cobalt(II) or cobalt(III) can be derived by appropriate choice of solvent or medium.

$Co^{II}Co^{I}$ is observed in inflexible binuclear cobalt phthalocyanines; this mixed valence species has significant stability due to delocalization of the charge.

$Co^{III}Co^{II}$ is observed in inflexible binuclear phthalocyanines.

Pc(-2)Pc(-3) is observed in rigid main-group M-bridge-M species such as RSiPc-O-PcSR, but less readily obtained in flexible binuclear species.

There is every reason to expect that the above observations are fairly general and that most transition-metal ions would yield mixed-valence complexes in pillared phthalocyanine species. This study provides the foundation for future studies in mixed-valence phthalocyanine chemistry. It is possible to predict with some certainly the situations that should give rise to mixed-valence phthalocyanine chemistry and estimate the energetics thereof and hence to use this capability in a design sense for technological application.

Acknowledgment. We are indebted to the Natural Sciences and Engineering Research Council (Ottawa) and the Office of Naval Research (Washington, DC) for financial assistance. We thank Union Carbide (Parma) for the gift of highly oriented pyrolytic graphite.

Contribution from the Departments of Chemistry, Drexel University, Philadelphia, Pennsylvania 19104, University of Virginia, Charlottesville, Virginia 22901, and Memorial University of Newfoundland, St. John's, Newfoundland, Canada A1B 3X7

Analogues for the Specific Iron-Binding Site in the Transferrins: Molecular Structure of a Ternary Iron(III) Model Complex and Spectroscopic, Redox, and Reactivity Properties of Related Compounds

Michael R. McDevitt,[1a] Anthony W. Addison,*[,1a] Ekkehard Sinn,*[,1b] and Laurence K. Thompson[1c]

Received August 1, 1989

Small-molecule analogues of the specific iron-binding site of the iron tyrosinate protein lactoferrin have been prepared and characterized. The single-crystal X-ray structure of an *N*-methylimidazole adduct of one of these complexes, (2-(benzimidazol-2-ylmethyl)phenolato)(2-oxo-3-methylbenzoato)bis(*N*-methylimidazole)iron(III), has been determined by standard procedures and refined by least-squares methods to a conventional *R* factor of 0.061. The purple crystals belong to the orthorhombic space group *Pbca* with $Z = 8$ and unit cell dimensions $a = 17.470$ (5) Å, $b = 17.030$ (6) Å, and $c = 18.910$ (7) Å. The iron(III) complex has a pseudooctahedral N_3O_3 donor set, utilizing bidentate ligands to provide phenolate, benzimidazole, and carboxylate coordination to mimic respectively the known tyrosinate, histidine, and aspartate protein side chains. The model complexes, which do not include any severe steric constraints, mimic several features of the transferrins: (i) tyrosinate-to-iron(III) charge-transfer band wavelength and molar absorptivity; (ii) reactivity with cyanide to produce a low-spin iron(III) adduct; and (iii) a quite negative value of $E_{1/2}$. The relationship between these analogues and the active sites of the transferrins is discussed in light of these results.

Introduction

The transferrins (serum transferrin, lactoferrin, and ovotransferrin) are an important subclass of iron(III) tyrosinate proteins[2] that reversibly bind 2 mol of iron(III) cooperatively with 2 mol of carbonate or bicarbonate.[3] Inorganic coordination complexes designed to model the iron active site in transferrin[4-8]

(1) (a) Drexel University. (b) University of Virginia. (c) Memorial University of Newfoundland.

(2) Que, L., Jr. *Coord. Chem. Rev.* **1983**, *50*, 73.
(3) Chasteen, N. D. *Coord. Chem. Rev.* **1977**, *22*, 1.

0020-1669/90/1329-3425$02.50/0